

Design of Compliant Mechanisms for Morphing Structural Shapes

KERR-JIA LU* AND SRIDHAR KOTA

Department of Mechanical Engineering, University of Michigan, Ann Arbor, MI 48109-2125, USA

ABSTRACT: Various compliant mechanism synthesis methods have been developed over the past decade; however, very little attention has been directed towards adaptive shape change problems. In this paper, we present a systematic method for synthesizing compliant mechanisms to morph a given curve or profile into a target curve utilizing minimum number of actuators (typically one). Two objective functions are formulated, using Least Square Errors and a modified Fourier Transformation, to capture the shape differences. The topology and dimensions of the optimal compliant mechanism are generated using Genetic Algorithms. Applications of this synthesis approach are demonstrated through two adaptive antenna design examples.

Key Words: compliant mechanism, shape morphing, genetic algorithm, adaptive structure, structural optimization

INTRODUCTION

A compliant mechanism is a single-piece flexible structure that delivers the desired motion by undergoing elastic deformation as opposed to the rigid body motions in a conventional mechanism (Kota et al., 1999). It is designed to accomplish with a one-piece device what conventional mechanisms can do with multiple pieces. It is designed to be flexible enough to transmit motions, yet stiff enough to withstand the external loads. The hingeless nature of compliant mechanism eliminates the backlash error and effectively reduces the production and maintenance costs associated with the multiple piece assembly. Moreover, the distributed compliance throughout the compliant mechanism provides a smooth deformation field, which reduces the stress concentration. These features are particularly attractive when dealing with applications such as shape change in aircraft wings and antenna reflectors. These systems generally require a reduced system weight, accurate and smooth surface shapes, and simple control schemes that compliant mechanisms can offer.

Various systematic strategies for compliant mechanisms, using a structural optimization approach, have been developed in the past decade to fulfill various functional requirements, such as maximizing energy efficiency (Hetrick and Kota, 1999) or maximizing geometric advantage (Joo et al., 2001). These synthesis approaches have been successfully applied to the design

of MEMS motion amplifiers and compliant grippers. Previous research on compliant mechanism synthesis has typically employed a two-step synthesis approach as shown in Figure 1 (Joo, 2001): (a) topology synthesis; then (b) size and geometry optimization. The topology and dimensional aspects of an elastic body is illustrated in Figures 2 and 3; given a one-piece elastic body, the topology is defined by the number of interior holes and their locations with respect to the boundary conditions (loading and support locations), while the dimensions of the remaining material is determined by the size and shapes of these holes. The two-step approach decomposes the interrelated topology and dimensional syntheses into two separate stages: the topology synthesis ensures the motion in the desired output direction (a quality aspect); the size and geometry optimization refines the mechanism dimensions to achieve a desired objective, such as maximizing displacement (a quantity aspect). Research has suggested that the decomposition can simplify the problem and yield successful results in real single-input single-output (SISO) applications (Ananthasuresh et al., 1994; Frecker, 1997; Hetrick and Kota, 1999; Joo et al., 2001).

Although various methods for synthesizing compliant mechanisms have been developed in the past decade, very little attention (Saggere and Kota, 1999) has been directed to problems related to shape change. Unlike the SISO problems studied in most of the previous research, the quality of the solutions to the shape change problems depends greatly on the precise deformation (direction and magnitude) of all or several discrete output points along the shape-changing boundary. With

*Author to whom correspondence should be addressed.
E-mail: kjlu@umich.edu.

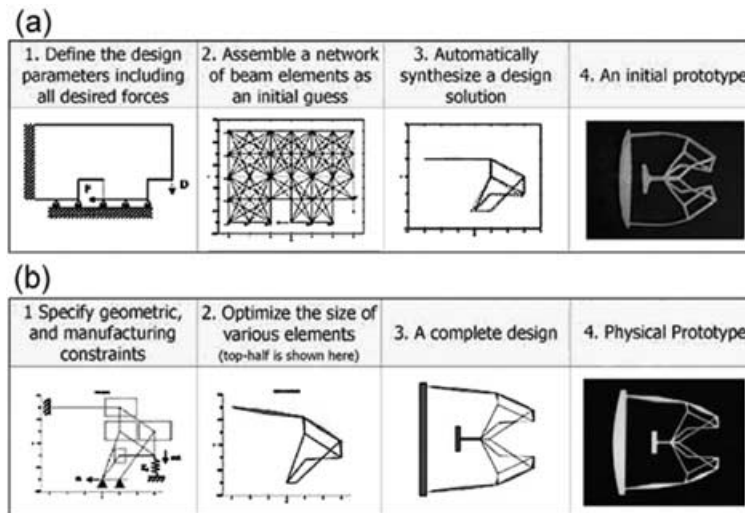


Figure 1. Typical compliant mechanism synthesis involves a two-step approach, where the topology is optimized first, and with the optimized topology as an input, the optimal dimensions for the compliant mechanism are determined in the second step (Joo, 2001): (a) topology synthesis; (b) dimensional synthesis.

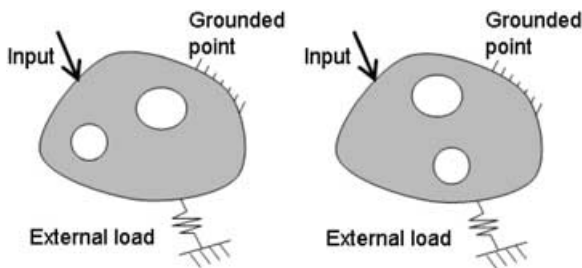


Figure 2. Two elastic bodies with different topologies.

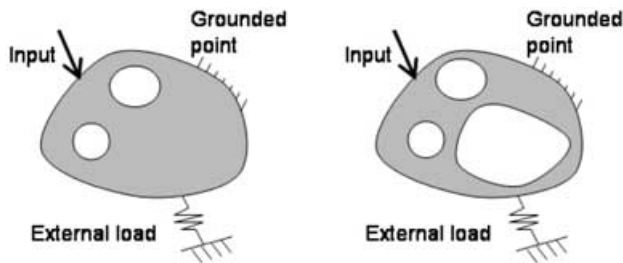


Figure 3. Two elastic bodies with different topology and dimensions.

multiple output points presented in these problems, it might be inappropriate to use the two-step approach that focuses on the performance of only one particular output point. Since the deformation of the shape-changing boundary is simultaneously influenced by the topology and dimensions of the compliant mechanism, it is critical to unify the two synthesis steps and address them simultaneously. Furthermore, previous research on topology synthesis has employed continuous optimization methods to find the optimal material distribution by eliminating unnecessary elements from the initial element network (Figure 1(a)-2). However, the elimination or preservation of elements is, in fact, a discrete decision, and it should be addressed using discrete

variables. Therefore, the objective of this research is to develop a generalized scheme to synthesize compliant mechanisms that can morph one shape to another desired shape with minimum error. In addition, discrete and continuous variables should be used simultaneously in this unified synthesis approach to determine the topology and dimensions of the compliant mechanism.

SHAPE CHANGE USING COMPLIANT MECHANISMS

The performance of many mechanical-structural systems, such as aircraft wings and antenna reflectors, is directly related to the geometric shapes of their components. Such systems require different shapes for different operating conditions, but they are generally designed to have one fixed shape that constitutes a compromise with respect to all the operating conditions. To respond to varying operating conditions and external disturbances, the component shape has to change adaptively to maintain optimal system performance and enhance versatility. Various adaptive shape change (shape morphing) systems have been developed and incorporated into practical applications (Austin and Van Nostrand, 1995; Washington, 1996; Austin et al., 1997; Martin et al., 1997, 1998, 2000; Yoon and Washington, 1998; Webb et al., 1999; Yoon et al., 2000; Ameduri et al., 2001; Angelino and Washington, 2001). Most of these shape morphing systems involve the use of smart actuators and materials, such as shape memory alloys (SMAs) and lead zirconate titanate (PZT). Although the smart actuators can provide light-weight actuation schemes, their scalability is uncertain when realistic scale problems are considered. A compliant mechanism, on the other hand, changes

its shape through the structural deformation, which is independent of the scale of the problem, thus offering an alternative means to achieve a desired shape change. In this research, we will investigate the feasibility of this alternative shape change method and explore its potential benefits.

Figure 4 gives a simple illustration of how a compliant mechanism changes its shape. The actuator provides a displacement or force input to the system, and the compliant mechanism deforms due to the structural flexibility, which, in turn, changes the boundary from its initial state (initial curve profile) into a deformed state (deformed curve profile). In this research, it is assumed that the compliant mechanism is composed of frame-like elements, where the structural deformation comes mainly from bending of the beams. The goal is to find the optimal topology and dimensions for the compliant mechanism, so that the deformed curve profile, due to input actuation, matches the target curve with minimum error. Although Figure 4 only illustrates the shape morphing between two curves using a two-dimensional planar compliant mechanism, it can be regarded as one cross-section of a shape morphing surface, such as an aircraft wing cross-section along the wingspan. More complicated three-dimensional surface shape change can be explored in the future by expanding the synthesis method developed in this research, but the scope of this paper will be restricted to the design of two-dimensional compliant mechanisms. Several additional assumptions also include: (1) the shape-changing object will change from its initial profile to only one target profile; (2) the initial and target profiles are specified a priori; (3) the shape-changing object is integrally attached to the compliant mechanism; and (4) the compliant mechanism has only a single external input actuator at a specified location. The actuator can be selected from a variety of ranges and types, such as electric motor or even the smart actuators, as long as the required motion and force can be provided. The shape change concept can be applied to many engineering fields in various scales,

such as aircraft wings, antenna reflectors, lumbar support, or fluid flow control devices. Two antenna shape change examples will be shown later to illustrate the synthesis approach developed in this research.

METHODOLOGY

This paper presents a systematic synthesis approach for compliant mechanisms that can achieve the desired shape change from an initial curve profile to a target one. The problem specifications include the initial and target curve profiles, support locations, external loads, actuator type and location, available design domain, and material properties. As can be seen from the flowchart in Figure 5, the synthesis approach starts with a feasibility check to ensure the shape change is attainable. The next step is to

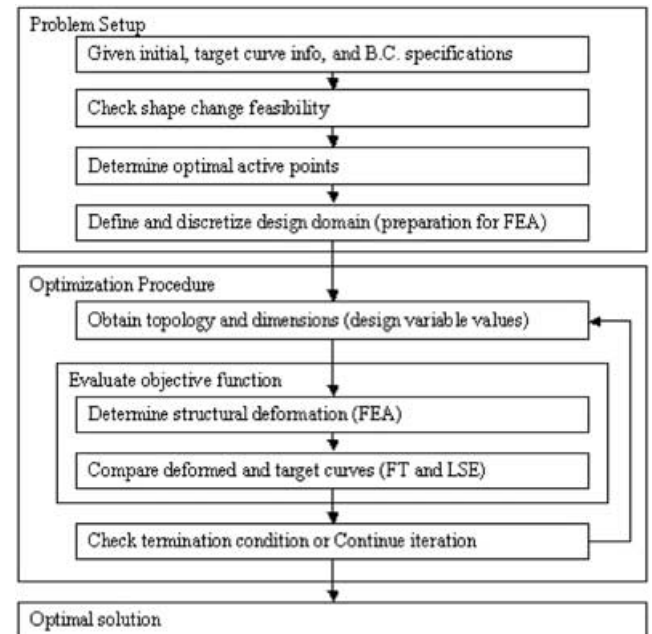


Figure 5. Flowchart for the compliant mechanism synthesis approach.

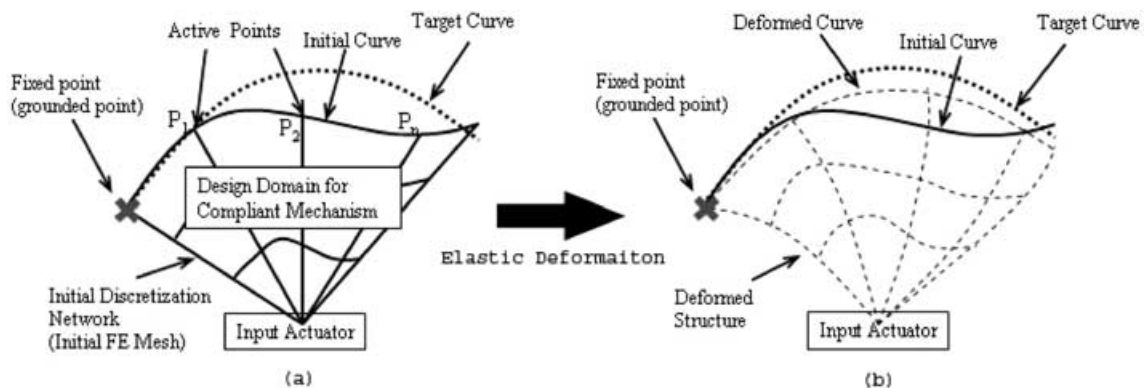


Figure 4. An illustration for a shape change compliant mechanism: (a) shows the problem specifications and how the input actuator is connected to the active points; (b) shows the deformed structure with its deformed curve boundary and how that compares to the target curve.

discretize the design domain into an initial grid, and the grid nodes are connected with beam elements to form an initial finite element mesh. This initial mesh then goes through an optimization process that searches for the optimal topology and dimensions of the compliant mechanism. In this optimization process, the objective is to minimize the error between the deformed and target curve. A finite element analysis (FEA) is used to solve for the deformed boundary shape, which is, then, compared to the target curve profile to define the shape change error. Due to the mixed variable types from the topology (discrete) and dimensions (continuous), a genetic algorithm (GA) is adopted to simultaneously determine the optimal topology and dimensions of the compliant mechanism. The steps in this synthesis procedure are described in detail in the following sub-sections.

Problem Setup – Check Shape Change Feasibility

A preprocessor first examines the given initial and target curves in order to evaluate if the shape change is attainable. The initial curve is assumed to be stress free before the shape change and to have a constant rectangular cross-section. The nominal dimensions of the cross-section are the minimum feature sizes from the manufacturing constraints. The feasibility check then estimates the maximum stress along the curve when it is deformed into the target shape. The maximum stress is checked against yielding with two criteria: (1) the stress due to axial tension or compression must be smaller than yielding stress; and (2) the stress due to bending must be smaller than yielding stress. For the first criterion, the preprocessor calculates the length of both curves (initial and target), and estimates the axial stress that is required to stretch or compress the curve from its initial length to the target one. For the second criterion, the preprocessor first calculates the curvature functions of both curves, $\kappa_{\text{INI}}(l)$ and $\kappa_{\text{TAR}}(l)$, where l is the normalized arc length varying from 0 to 1. The curvature difference function, $d\kappa(l)$, is then defined in Equation (1) as the difference between the two curvature functions. This can be considered as the local curvature change along the curve. Since the bending stress along a beam is proportional to its local curvature change, according to Euler–Bernoulli beam theory, the maximum bending stress can be calculated from the curvature difference function as shown in Equation (2). If both of the maximum stresses due to axial tension and bending stay within the yielding limit of the selected material, the shape change is considered feasible, and the algorithm invokes the next step in the synthesis procedure.

$$d\kappa(l) = \kappa_{\text{INI}}(l) - \kappa_{\text{TAR}}(l) \quad (1)$$

$$\sigma_{\text{max}} = \frac{Eh}{2} \max(d\kappa(l)) \quad (2)$$

where $\kappa_{\text{INI}}(l)$ and $\kappa_{\text{TAR}}(l)$ are the curvature functions of the initial and target curves; l is the normalized arc length; E is the Young's Modulus; h is the beam height (in-plane dimension).

Problem Setup – Determine Optimal Active Points

Once the problem passes the feasibility check, the design domain is parameterized so that the designs can be described in terms of the design variables that will be incorporated into the optimization process in the later stage of the synthesis process. Previous research has been using an initial finite element mesh to discretize the design domain either with two-dimensional quadrilateral elements or with a grounded structure consists of beam/truss element network (Figure 1(a)-2). The design variables are then defined as the dimensions of the elements, such as the cross-section areas. The discretization mesh size is typically pre-specified by the designer without any clear guideline on the size selection. Although finer mesh can generate results with higher resolution, it also increases the number of design variables required to represent a design. In this research, we want to gain some insight into the required complexity of the initial discretization element network by studying the curve profiles before and after the shape change.

It is assumed that the shape change boundary is connected to the interior elements of the compliant mechanism through several ‘active points,’ such as P_1 , P_2 , and P_n in Figure 4. The compliant mechanism can then transmit the input actuation motion through these active points to control the motion/shape of the morphing boundary (the adaptive surface). Hence, the active points can also be regarded as the ‘output points’ of the (interior) compliant mechanism. The shape change can be achieved with minimum error if we have full control of every point along the curve, but designing a compliant mechanism with so many output points (active points) might involve a tremendous number of design variables. It is, thus, important to identify the minimum number of required active points, such that, when they are connected to the interior elements, the whole compliant mechanism can achieve the desired shape change with acceptable error.

To determine the active point locations, a piecewise linear function is used to approximate the curvature difference function, $d\kappa(l)$, and the active points are defined as the end points of each linear section. The curve fitting function is piecewise linear because the curvature distribution is linear for a straight beam with constant cross-section, subjected to uniform pressure loads or end loads. The morphing boundary can be regarded as several beam segments connected in series with the interior compliant mechanism applying

(transmitting) forces/moments to the end points of each segment (active points). An optimization process is then used to determine the minimum number of active points while constraining the curve fitting error below an acceptable tolerance, ε . They are shown in Equations (3) and (4) as the objective function and the constraint. The binary design variable, activePt_i , represents the i^{th} given data point along the shape change boundary; the i^{th} data point becomes an active point only if $\text{activePt}_i = 1$. A GA (Goldberg, 1989) is employed to find the optimal number of design variables, because the binary variables can be easily incorporated in the GA. The optimal locations of the active points can be obtained from the optimal activePt vector; the j^{th} data point on the shape change boundary is considered an optimal active point location if $\text{activePt}_j = 1$. More details on GA will be described later in this paper.

$$\min_{\text{activePt}_i} \left(\sum_{i=1}^n \text{activePt}_i \right) \text{ Minimize number} \quad (3)$$

of active points

Subject to

$$g1 : |d\kappa(l_i) - d\kappa^*(l_i)| \leq \varepsilon \quad \text{Curve fitting} \quad (4)$$

error constraint

where n is the number of given data points along the shape change boundary; $\text{activePt}_i \in \{0, 1\}$; $d\kappa(l)$ is the curvature difference function; $d\kappa^*(l)$ is the piecewise linear function connecting $(l_j, d\kappa(l_j)) \in \{j | \text{activePt}_j = 1\}$; and ε is the acceptable fitting error.

Problem Setup – Discretize Design Domain and Define Design Variables

After obtaining the locations of the active points, the preprocessor proceeds to discretize the design domain and define the topology and dimensional design variables for the compliant mechanism optimization in the next step. As shown in Figure 4, the design domain is defined by the initial curve and the input actuator location, considering space constraints and boundary condition specifications as well. Based on the active points and boundary conditions, the design domain is then discretized into an initial grid, where grid nodes are connected with beam elements to form an initial discretization network. With a given initial grid, the initial element network provides many possible topologies for the final solution simply by removing or including different elements within this network. An optimization procedure can then be used to determine the best topology among them in the later stage of this synthesis approach. This is similar to the grounded

structure approach seen in previous research (Figure 1(a)-2), but instead of discretizing the design domain with arbitrary grid size, the grid size in one direction is now determined by the active points. The grid size in the other direction and the configuration of the initial network are selected based on the problem specification and engineering experience to form a variety of available configurations. It is shown later that the selection of initial element network is critical to the resulting optimal solution.

After creating the initial element network, two design variables are assigned to each beam element to describe the compliant mechanism topology and the dimensions of each beam segments. In this research, each beam element connecting any two grid nodes is assumed to have a constant rectangular cross-section. The in-plane beam dimensions (beam heights) are considered the dimensional design variables, while the out-of-plane dimensions (beam widths) are prescribed to be constant for all elements. As shown in Equations (5) and (6), for the i^{th} beam element, it is assigned a binary variable ($h\text{Top}_i$) and a continuous real variable ($h\text{Dim}_i$) to represent the topology and dimension respectively. The final beam heights, h_i , are simply the multiplication of the two variables, expressed in Equation (7). It is also assumed that the shape change boundary always ‘exists’ and has a constant in-plane dimension, $h\text{Boundary}$. Therefore, for an initial discretization mesh with n elements, there will be a total of $2n + 1$ design variables, including n binary topology variables, n continuous dimensional variables, and one continuous variable for the in-plane dimension of the shape change boundary. An optimization process is then incorporated to find the optimal values for these design variables, so that the desired shape change can be achieved with minimum error.

$$h\text{Top}_i \in \text{binary values (0: element eliminated,} \quad (5)$$

1: element remains)

$$h\text{Dim}_i \in \text{positive real numbers} \quad (6)$$

$$h_i = h\text{Top}_i \times h\text{Dim}_i, \quad (7)$$

where $i = 1, 2, \dots$, number of elements

Optimization Procedure – Optimization Method

An optimization problem is formulated at this point in order to find the optimal compliant mechanism that changes the initial curve into a target shape with minimum error. In this work, we use a GA to search for the optimal design, because it can search for a wider range of solution space (compared to local search), and it is capable of handling mixed design variables

(discrete + continuous). It also has a simple binary encoding data structure that enables the binary topology variables to be incorporated in GA naturally.

The GA is a heuristic optimization method that simulates the selection scheme found in nature, based on the principle of ‘survival of the fittest.’ The design variables are encoded into a chromosome string analogous to the genes on the DNA. It starts with a randomly generated population of individuals (designs), and subsequent new generations are created through a reproduction process. The chance of survival for one individual depends on its fitness value evaluated from the objective function defined in the optimization problem. The individual with higher fitness value has a higher chance to reproduce, but inferior ones can still survive with a lower probability to preserve the variety in each generation. Reproduction repeats until reaching the maximum number of generations, and the fittest design in the final generation is then considered the ‘optimal’ solution. GA allows solutions to jump from one local region to another in the solution space through the genetic operations, thus preventing the solution from being trapped in a local optimum. This also implies that the solution obtained from GA is independent of starting point, as opposed to that obtained from gradient-based continuous optimization methods. Although global optimum is still not guaranteed, GA gives a wider range of possible optimal solutions and is ‘more likely’ to find the global optimum. Details regarding GA can be found in the reference (Goldberg, 1989). In this paper, we will only highlight some important issues in GA, such as the encoding of chromosome string and the reproduction operation.

To utilize GA in this research, the topology and dimensional design variables are encoded into a chromosome string shown in Equation (8). The GA randomly creates a population of designs in the first generation, and successive generations are generated through the reproduction scheme, including selection, crossover, and mutation. The selection scheme is based on the fitness value of each design, which is the ‘deviation’ or ‘shape difference’ between the deformed and target curves. The deviation evaluation will be described in more detail in the next section when defining the objective function. As shown in Equations (9)–(12), using a roulette wheel selection scheme, two parent chromosomes ($p1$ and $p2$) are selected from the parent generation, and two new chromosomes ($k1$ and $k2$) are then created through genetic operations on $p1$ and $p2$. The crossover operation is done through exchanging part of the chromosome strings of the parents; the vertical lines in Equations (9) and (10) indicate the point of crossover, while the underline portions in Equations (11) and (12) show the segments of chromosome strings coming from the other parent. Note that the crossover point can be anywhere within

the chromosome code, including the topology and dimensional variables. The mutation for each new design, following the crossover, is simply defined by replacing an arbitrary value (any $hTop_i$, $hDim_i$, or $hBoundary$) in the chromosome string with a randomly generated value.

$$\text{design}(k) = \left[\begin{array}{c} \underbrace{h_k \text{Top}_1, \quad h_k \text{Top}_2, \quad \dots \quad h_k \text{Top}_n}_{\text{Topology}} \\ \underbrace{h_k \text{Dim}_1, \quad \dots \quad h_k \text{Dim}_n, \quad h_k \text{Boundary}}_{\text{Dimensions}} \end{array} \right] \quad (8)$$

where $k = 1, 2, \dots$, number of individuals in one generation; $n = \text{total number of beam elements}$; $hTop_i$ and $hDim_i$ are the topology and dimensional values for the i^{th} beam element.

$$p1 = \left[\begin{array}{c} h_1 \text{Top}_1, \quad \dots \quad h_1 \text{Top}_n, \quad h_1 \text{Dim}_1, \quad \dots \quad h_1 \text{Dim}_k \\ \hline h_1 \text{Dim}_{k+1}, \quad \dots \quad h_1 \text{Dim}_n, \quad h_1 \text{Boundary} \end{array} \right] \quad (9)$$

$$p2 = \left[\begin{array}{c} h_2 \text{Top}_1, \quad \dots \quad h_2 \text{Top}_n, \quad h_2 \text{Dim}_1, \quad \dots \quad h_2 \text{Dim}_k \\ \hline h_2 \text{Dim}_{k+1}, \quad \dots \quad h_2 \text{Dim}_n, \quad h_2 \text{Boundary} \end{array} \right] \quad (10)$$

$$k1 = \left[\begin{array}{c} h_1 \text{Top}_1, \quad \dots \quad h_1 \text{Top}_n, \quad h_1 \text{Dim}_1, \quad \dots \quad h_1 \text{Dim}_k \\ \hline h_2 \text{Dim}_{k+1}, \quad \dots \quad h_2 \text{Dim}_n, \quad h_2 \text{Boundary} \end{array} \right] \quad (11)$$

$$k2 = \left[\begin{array}{c} h_2 \text{Top}_1, \quad \dots \quad h_2 \text{Top}_n, \quad h_2 \text{Dim}_1, \quad \dots \quad h_2 \text{Dim}_k \\ \hline h_1 \text{Dim}_{k+1}, \quad \dots \quad h_1 \text{Dim}_n, \quad h_1 \text{Boundary} \end{array} \right] \quad (12)$$

Optimization Procedure – Objective Function for Curve Comparison

To evaluate the performance of a design, the associated fitness value is evaluated using a curve comparison scheme that captures the shape differences between the deformed and target curves. For each compliant mechanism defined by a chromosome string, a FEA is used to solve for the structural deformation. The deformed curve profile is then extracted from the deformed structural boundary and compared to the desired target curve. The deformed and target curves are expressed in terms of two sets of sampling points that are evenly distributed along the curve lengths, as shown in Figure 6.

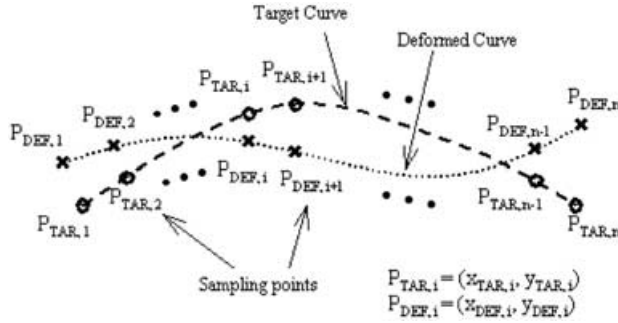


Figure 6. Sampling points on the deformed and target curves.

Previous research (Saggere and Kota, 1999) defined the ‘deviation’ between the deformed and target curves as the average Euclidian distance between the two curves at the sampling points. This is termed as the least square error (LSE) deviation and shown in Equation (13).

$$\text{deviation}_{LSE} = \frac{1}{n} \sum_{i=1}^n \sqrt{(x_{DEF,i} - x_{TAR,i})^2 + (y_{DEF,i} - y_{TAR,i})^2} \quad (13)$$

Since LSE deviation compares the differences between all sampling points along the curve, the scale, orientation, and shape information are captured and can potentially lead to a solution that matches the target curve exactly. But this might discard a portion of possible solutions when there is symmetry in the problem. Figure 7(a) shows an example that changes a symmetric curve (about y -axis) into a curve that bends towards the right. Assuming that Figure 7(b) is a solution to this problem, it can be seen that Figure 7(c) can also be a valid solution simply by mirroring the solution about y -axis, but this solution can be discarded using LSE deviation. Figure 8 shows another shape change example where LSE deviation is inappropriate to describe the ‘shape’ difference. The goal is to deform a circle into an ellipse, but the ellipse can be in any orientation because the circle is axisymmetric. Using LSE deviation will prevent the algorithm from finding the solution in Figure 8(c). Therefore, for symmetric problems like these, it is necessary to use a curve comparison scheme that focus purely on the differences in ‘shape’ instead of the sampling point locations.

For situations emphasizing the shape difference, we use a modified Fourier Transformation (FT) to characterize and compare the curves. Standard Fourier Transformation is shown in Equation (14), where $f(t)$ is a periodic function in time-domain. It transforms the periodic function into its frequency content in terms of harmonic amplitudes and their corresponding frequencies, as shown in Figure 9. Lower frequency information dominates the overall signal shape, while higher frequency information usually contributes to finer

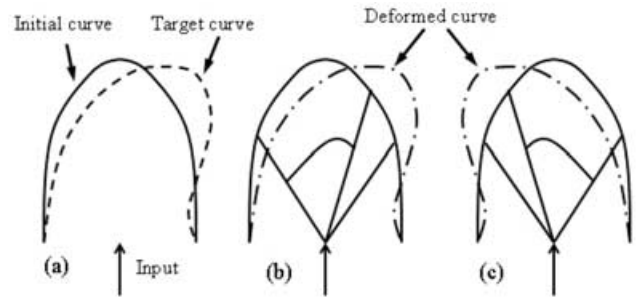


Figure 7. (a) A shape change example: bending a symmetric curve (about y -axis) towards the right; (b) an example solution (not the actual solution) to this problem; (c) a mirror image solution which could be discarded during the optimization process using LSE.

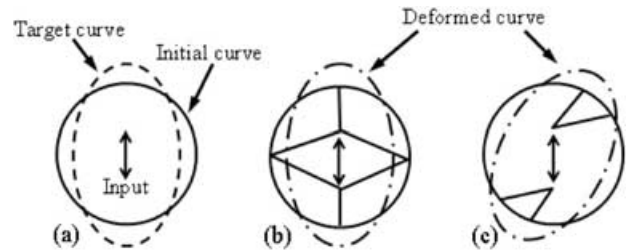


Figure 8. (a) A shape change example that changes a circle into an ellipse; (b) a design with deformed curve that matches the target curve exactly (shape and locations); (c) a design that can achieve shape change from a circle to an ellipse at an angle.

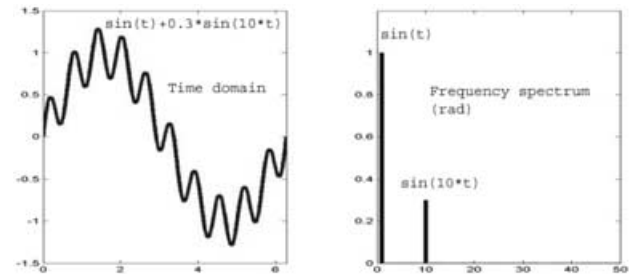


Figure 9. A one-dimensional periodic signal and its frequency spectrum from the Fourier Transformation. Lower frequencies dictate the overall shape, while higher ones describe the finer details.

features. This is especially useful for the curve comparison task not only because the information is purely about the shape, but it also provides shape information of different importance level.

$$F(\omega) = \mathcal{F}\{f(t)\} = \int_{-\infty}^{\infty} f(t)e^{-j\omega t} dt \quad (14)$$

To utilize FT, the curve has to be represented as a one-dimensional periodic signal. One way to achieve this setting is to express the curve shape in terms of its location in Y -direction as a function of its arc length. Since the start and end points of the curve do not necessarily have the same value in global Y -direction, the sampling points on the curve have to go through a coordinate transformation from the original global X - Y coordinates to the x' - y' coordinates, where the x' -axis is

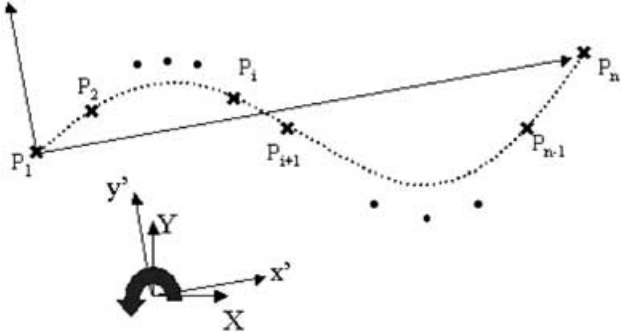


Figure 10. The coordinate transformation used in the modified FT method, so that the deformed and target curves can have the same value (in the y' -direction) at the starting and end points.

determined by connecting the start and end points of the curve, as shown in Figure 10. The curve is then expressed as a function of the arc length, hence, a one-dimensional periodic signal. Instead of using FT directly, the curve in the new coordinates and parameterization is approximated using Discrete Fourier Transformation (DFT), because the exact function of the curve is unknown. The DFT takes discrete sampling information on the curve and approximates the curve with discrete frequencies and their corresponding harmonic amplitudes, that is, the Fourier Descriptors (FDs). To further accelerate the calculation speed, Fast Fourier Transformation (FFT) can be used instead of DFT by resampling the modified curve (arc length vs. y' -direction value) with 2^N points, where N is an integer.

To evaluate the deviation between the deformed and target curves, the modified FT (coordinate transformation + FFT) is used to describe both of the curves separately, resulting in two sets of FDs. As shown in Figure 11 and Equation (15), the sum of amplitude differences at corresponding frequencies is then defined as the FT deviation between the two curves.

$$\text{deviation}_{\text{FT}} = \sum_{k=1}^{n\text{Amp}} |\text{AmpTAR}_k - \text{AmpDEF}_k| \quad (15)$$

Where AmpTAR_k and AmpDEF_k are the k^{th} harmonic amplitudes for the target and deformed curves respectively, and $n\text{Amp}$ is number of amplitudes (number of resampling points).

As shown in Equation (16), either of the two deviation measures (LSE or FT) can be used as the objective function in the optimization procedure, depending on the nature of the problem. The structural deformation is obtained from FEA, as indicated in Equation (17). All the beam elements are subjected to size constraints, shown in Equations (18) and (19). The stiffness constraint shown in Equation (20) limits the maximum deformation on the shape change boundary before activating the input actuator. A stress constraint

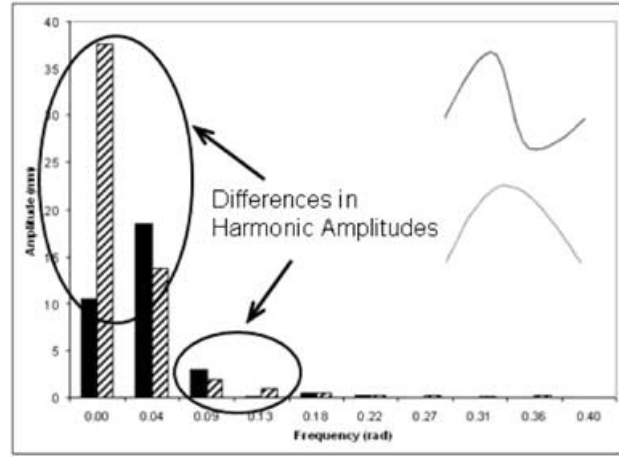


Figure 11. An example of the differences in harmonic amplitudes for two curves.

Equation (21) is also applied to all elements to prevent structural failure. The optimization model can, thus, be summarized in the following.

Objective Function

$$\min_{\substack{h\text{Top}_i, h\text{Dim}_i \\ h\text{Boundary}}} (\text{deviation}_{\text{LSE}}) \quad \text{or} \quad \min_{\substack{h\text{Top}_i, h\text{Dim}_i \\ h\text{Boundary}}} (\text{deviation}_{\text{FT}}) \quad (16)$$

Subject to

$$g1 : \mathbf{d} = \mathbf{K}^{-1}\mathbf{F} \quad \text{FEA equilibrium} \quad (17)$$

$$g2 : h\text{Dim}_{\min} < h\text{Dim}_i \leq h\text{Dim}_{\max} \quad \text{size constraint} \quad (18)$$

$$g3 : h\text{Dim}_{\min} < h\text{Boundary}_i \leq h\text{Dim}_{\max} \quad \text{size constraint} \quad (19)$$

$$g4 : \max(d_j) \leq d_{\text{allow}} \quad \text{stiffness constraint} \quad (20)$$

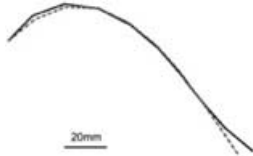
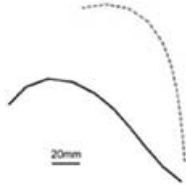
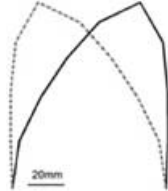

$$g5 : \sigma_i \leq \sigma_{\text{allow}} \quad \text{stress constraint} \quad (21)$$

$$g6 : h_i = h\text{Top}_i \times h\text{Dim}_i \quad \text{mixed variables}$$

$h\text{Top}_i \in \{0, 1\}, h\text{Dim}_i \in \mathbb{R}^+, i \in$ all beam elements, and $j \in$ degrees of freedom of nodes on the shape change boundary

For each chromosome string, the fitness value is evaluated using the objective function, and the best design in each generation is recorded throughout the evolution process. The reproduction process repeats until reaching the maximum number of generations, hence, terminating the evolution process. The optimal solution will be the best solution across all generations.

Table 1. Several test shapes and their corresponding LSE and FT deviation values.

Test1	Test2	Test3	Test4
			
LSE dev: 2.57 mm FT dev: 5.01 mm	LSE dev: 51.97 mm FT dev: 5.01 mm	LSE dev: 13.72 mm FT dev: 0 mm	LSE dev: 11.52 mm FT dev: 51.33 mm

VALIDATION OF OBJECTIVE FUNCTION

To examine how the LSE and FT deviations explore different aspects of shapes, the deviation measures defined in Equations (13) and (15) are applied to several test shapes, shown in Table 1. The curve set in Tests 1 and 2 are the same, but the dash curve is translated and rotated with respect to the solid curve. Thus, FT deviation has the same values for the two cases (same shape), but LSE gives a large deviation value in Test 2 due to the location difference. Test 3 shows two curves that are mirror images of each other, so the FT deviation is zero while LSE deviation gives a large value. Test 4 shows that when two curves have very different shapes, both LSE and FT have large deviation values, but FT captures the shape difference better.

DESIGN EXAMPLES

Recent studies (Washington, 1996; Martin et al., 1998, 2000; Yoon and Washington, 1998; Yoon et al., 2000; Angelino and Washington, 2001) have shown that antenna reflector adaptation can potentially enhance system performance and increase flexibility, such as changing the signal pattern or coverage area. Two examples similar to the ones shown in Washington (1996) are presented in this section to illustrate the synthesis approach described in this paper and demonstrate the feasibility of shape change using compliant mechanisms.

Antenna Reflector – Beam Shaping

Figure 12 is an example of antenna reflector in its beam-shaping mode that changes the focus of the reflector to vary the radiation pattern. In this example, we design a compliant mechanism that is capable of changing the parabolic curve (initial curve) into a circular curve (target curve). Due to symmetry about the y -axis, only the left half of the reflector is modeled. The data points along the initial and target curves are

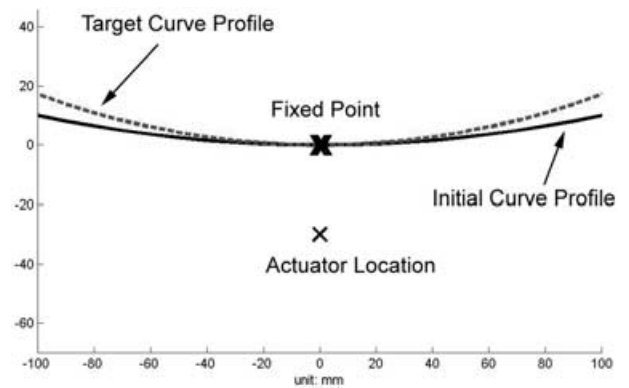


Figure 12. An antenna reflector that changes from a parabolic shape into a circular shape.

listed in Table 2. As shown in Figure 12, displacement input of 5 mm in the y -direction is located at $(0, -30)$, and a fixed point is located at $(0, 0)$. Multiple external loads of -1 N are applied to the reflector surface. The design domain is then defined by connecting the input, fixed point, and the initial curve. Using ABS plastic (Acrylonitrile–butadiene–styrene: Young's Modulus = 2480 MPa, Yield Stress = 34.45 MPa) as the material, the estimated maximum axial stress and bending moment are both below the yielding limit of ABS, thus the shape change is feasible. The curvature functions ($\kappa_{INI}(l)$ and $\kappa_{TAR}(l)$) and curvature difference function ($d\kappa(l)$) are shown in Figure 13. After the active points are determined using GA, an initial discretization network are created as in Figure 14 by connecting the actuation location to the optimal active points along the boundary with a beam element mesh. The horizontal element members are included to provide stiffness or alternative paths between input and the active points.

To search for the optimal topology and dimensions for the compliant mechanism, the LSE deviation objective function is used in this example, because both the initial and target curves are asymmetric in the half-model. The out-of-plane beam dimension is specified as 4 mm, and the in-plane dimension is allowed to

Table 2. Information of the data points along the initial and target curves in the beam shaping example.

Data point No.	Initial Curve (x, y) (mm)		Target Curve (x, y) (mm)	
1	-100.0000	10.0000	-100.0000	17.1573
2	-90.3321	8.1599	-90.3321	13.9229
3	-80.5598	6.4899	-80.5598	11.0188
4	-70.6946	4.9977	-70.6946	8.4485
5	-60.7477	3.6903	-60.7477	6.2148
6	-50.7306	2.5736	-50.7306	4.3204
7	-40.6550	1.6528	-40.6550	2.7675
8	-30.5324	0.9322	-30.5324	1.5578
9	-20.3745	0.4151	-20.3745	0.6927
10	-10.1931	0.1039	-10.1931	0.1732
11	0.0000	0.0000	0.0000	0.0000

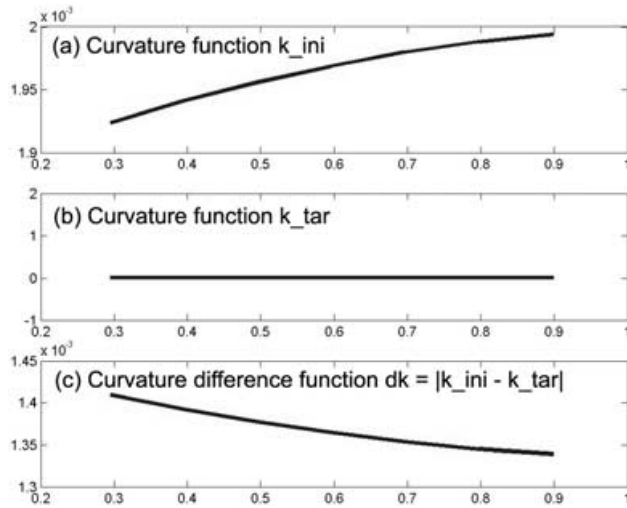


Figure 13. (a) The curvature function for the initial curve; (b) the curvature function for the target curve; (c) the curvature difference function for the beam shaping example shown in Figure 12.

vary between 1.5 and 4 mm. The GA starts with an initial population of 200 individuals and allows 50 generations, while the crossover and mutation probabilities are 0.8 and 0.4, respectively. The total CPU time for the optimization process is less than 15 min. As can be seen from the result in Figure 15, the optimized compliant mechanism can indeed achieve the desired shape change with the LSE error of only 0.4689 mm. It is also shown that the optimized topology is different from the initial element network in Figure 14, which implies that the topology and dimensions of the compliant mechanism are determined simultaneously.

Antenna Reflector – Beam Steering

Figure 16 is an example of antenna reflector in its beam-steering mode that changes the orientation of the reflector to vary the coverage area. In this example, we design a compliant mechanism that is capable of simulating a rotation of 2.86° (0.05 rad) clockwise about the center. The data points along the initial and

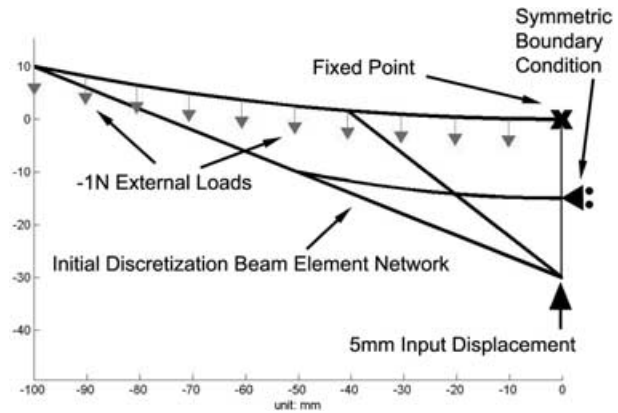


Figure 14. Initial discretization element network and boundary conditions are shown. Only half of the antenna is modeled due to symmetry.

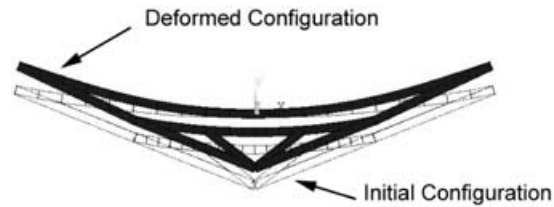


Figure 15. The optimized compliant mechanism with the deformed and target curves.

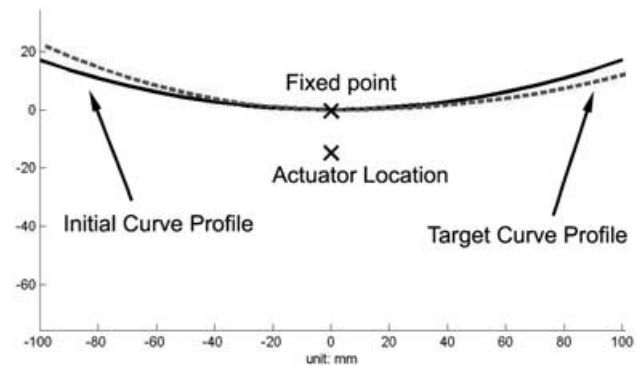


Figure 16. Two ends of the antenna reflector are required to bend upwards and downwards to simulate a change in orientation of 3° clockwise.

target curves are listed in Table 3. As shown in Figure 16, a displacement input of 1 mm is located at (0, -15), and a fixed point is located at (0, 0). Uniform external loads of -1 N downwards are again applied to the reflector surface. Following the same procedure in the previous example, the initial discretization network created by connecting the input and active points are shown in Figure 17.

Since the initial curve is symmetric about y-axis, FT deviation objective function is used in this example. In this example, the out-of-plane beam dimension is 4 mm and the in-plane dimension is allowed to vary between 2 and 4 mm. The GA starts with an initial population of 60 individuals and allows 20 generations, while the crossover and mutation probabilities are 0.8 and 0.5,

Table 3. Information of the data points along the initial and target curves in the beam steering example.

Data point No.	Initial Curve (x, y) (mm)		Target Curve (x, y) (mm)	
1	-70.6946	8.4485	-98.9249	22.1573
2	-60.7477	6.2148	-89.4997	18.1974
3	-50.7306	4.3204	-79.9410	14.5743
4	-40.6550	2.7675	-70.2573	11.3074
5	-30.5324	1.5578	-60.4582	8.4156
6	-20.3745	0.6927	-50.5551	5.9183
7	-10.1931	0.1732	-40.5614	3.8345
8	0.0000	0.0000	-30.4916	2.1827
9	10.1931	0.1732	-20.3623	0.9814
10	20.3745	0.6927	-10.1918	0.2481
11	30.5324	1.5578	0.0000	0.0000
12	40.6550	2.7675	10.1944	0.0983
13	50.7306	4.3204	20.3867	0.4040
14	60.7477	6.2148	30.5732	0.9329
15	70.6946	8.4485	40.7486	1.7005
16	80.5598	11.0188	50.9061	2.7225
17	90.3321	13.9229	61.0372	4.0140
18	100.0000	17.1573	71.1319	5.5896
19	-70.6946	8.4485	81.1786	7.4633
20	-60.7477	6.2148	91.1645	9.6484
21	-50.7306	4.3204	101.0751	12.1573

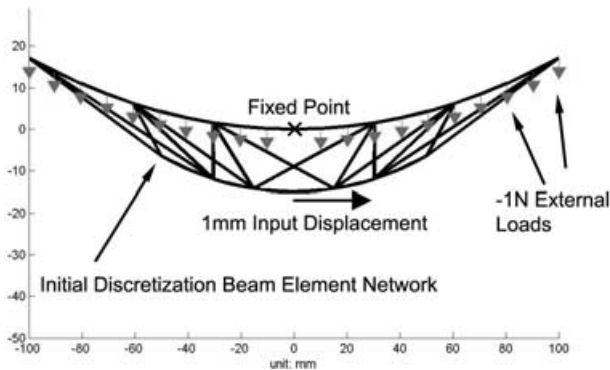


Figure 17. Initial discretization element network and input actuation.

respectively. The CPU time is less than 10 min. As shown in Figure 18, an interesting result that seemed to rotate in the opposite direction (counterclockwise) was obtained from the GA with the FT deviation of 1.1758 mm (LSE deviation of 6.0869 mm). This simply implies that the desired shape change can be achieved by mirroring the current design. The mirror image design is shown in Figure 19 with the same FT deviation value, but the LSE deviation is reduced to 0.6801 mm. This example suggests another useful aspect of the modified FT: when the actuation direction specified by the user does not allow the shape change in the ‘right’ direction, unlike the LSE which might prevent GA from finding a feasible solution, using the modified FT can help identify the mirror solution. Note that the FT deviation of 1.1758 mm is obtained after 20 generations. The

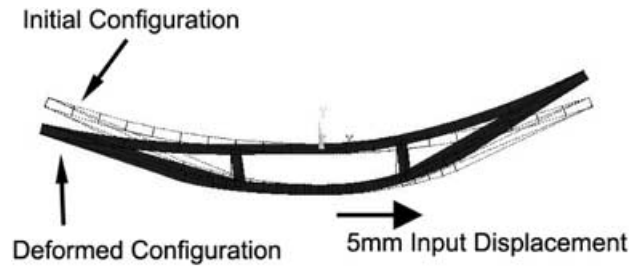


Figure 18. The optimized compliant mechanism for the beam steering mode.

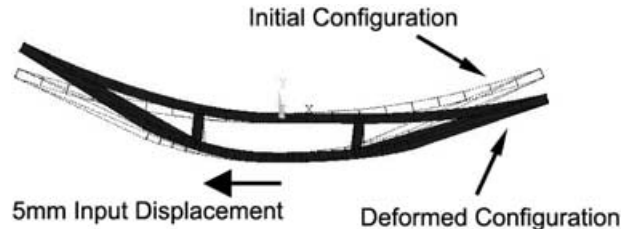


Figure 19. The mirror image design of the compliant mechanism shown in Figure 18.

deviation can be further reduced by adding more subsequent generations.

DISCUSSIONS

Determination of Active Points

In the problem setup step, the number and locations of active points are determined by fitting a piecewise linear curve through the curvature difference function, $d\kappa(l)$, assuming that all beam elements have uniform cross-section areas and that only uniform pressure loads or nodal loads are applied. However, if nonuniform distributed loads and cross-sections are used, $d\kappa(l)$ will no longer be piecewise linear; thus, a curve fitting process should be applied using a piecewise curve with a different order. For example, if linear varying distributed loads are presented, the moment along the element would be quadratic. Therefore, the active points will then be determined by finding a piecewise quadratic curve with minimum segments that fits $d\kappa(l)$ with minimum error. When using nonuniform cross-section elements, the same rule still applies, but it would involve a more complicated calculation.

Selection of Initial Discretization Mesh

In the problem setup step, the initial discretization mesh is created by interconnecting the input point, fixed points, active points, and some intermediate grid points within the design domain with a selected mesh configuration. In the later stage of the synthesis process, the

optimization toolbox searches for the optimal topology, which is the best connectivity among all possible solution (from the fully connected initial mesh). The resulting elements can be regarded as paths through which the input motion transfers to the output boundary (shape morphing boundary). The initial mesh lays the framework for many possible paths, while the GA searches for the optimal and necessary ones within all available paths. However, the grid size and mesh configuration (how grid points are connected), actually controls the size and complexity of the solution space, because selecting the initial mesh establishes the scope of all possible combinations of paths. Therefore, the initial mesh configuration is critical to the final result. Although the solution space of a more complicated initial mesh could include that of a simpler one, the computation time increases dramatically as the solution space gets larger. Thus, it is important to consider the trade-off between the complexity of the solution space and the available computation time. The majority of the previous research has been discretizing the design domain into arbitrary mesh size. In our work, the mesh is created by, first, connecting the input to the active points to create load paths from input to the output points. Some intermediate cross members, such as that shown in Figure 14, are then introduced by dividing the design domain between the input and the active points into several sections to provide structural stiffness. More complicated mesh configuration, such as including an 'X' in each grid box as shown in Figure 17, can also be used to exploit different solution space. Although the determination of cross members and mesh configuration is still somewhat arbitrary, we believe the use of active points is a definite improvement over existing approaches that discretize the entire design domain arbitrarily.

Specification of Boundary Conditions

The boundary conditions specified in this synthesis problem are critical to the final solution because the location/number of fixed points (grounded points) and location/direction of input can also change the solution space. With the same mesh configuration, the solution space complexity might be the same, but a different boundary condition (different locations of fixed points) would imply a completely different solution space (kinematically). Although the boundary conditions are specified at the beginning of the synthesis procedure, they can be not completely fixed throughout the optimization process in this research. When the element(s) connecting to a particular fixed point is(are) eliminated, the number and locations of the fixed points are changed. Thus, the synthesis problem is not confined to one particular set of boundary

conditions and is more likely to explore a larger variety of solutions.

Convergence of Genetic Algorithm

The GA used in this synthesis approach is a heuristic optimization technique that is independent of starting point and does not require sensitivity information. However, the computation time can be expensive when the number of design variables increases (with smaller grid size and more complex mesh type). If the neighborhood of the optimal solution is relatively small, compared to the entire solution space, it might encounter difficulties in even getting close into this neighborhood, let alone zeroing on the optimal solution. One way to accelerate the convergence speed is to employ a local search following the GA, or use a hybrid GA that includes some gradient information within the evolution process. The local search or gradient information can help converging to the local optimum, instead of jumping between different regions when using GA alone. On the other hand, the crossover and mutation operations in GA can be modified to better preserve the structure features than randomly switching elements between two designs.

CONCLUSION

We have developed a systematic synthesis approach for compliant mechanisms that are particularly focused to achieve adaptive shape change. The approach employs a discrete optimization scheme, GA, to explore the discrete nature of the topology, while simultaneously determining the dimensions for the compliant mechanism. In the optimization process, we have also included two different objective functions: LSE for asymmetric problems, and modified FT for symmetric ones. Two antenna shape change examples are then presented to demonstrate the feasibility of this approach. The results show that we can indeed achieve the desired shape change using compliant mechanisms and thereby realize the inherent benefits associated with them. More shape change examples are currently being studied to explore the limitation of this approach. Issues regarding the discretization mesh and GA convergence are also being investigated to refine the synthesis approach.

ACKNOWLEDGMENTS

Authors gratefully acknowledge the funding support of U.S. Air Force Office of Scientific Research for this work under the research contract number F49620-01-1-0160.

REFERENCES

- Ameduri, S., Esposito, C. and Concilio, A. 2001. "Active Shape Airfoil Control through Composite Piezoceramic Actuators," *SPIE Proceedings*, 4327:641–650.
- Ananthasuresh, G.K., Kota, S. and Kikuchi, K. 1994. "Strategies for Systematic Synthesis of Compliant Memes," *ASME Winter Annual Meeting*, 55:677–686.
- Angelino, M. and Washington, G. 2001. "Point Actuated Aperature Antenna Development," *Proceedings of SPIE*, 4334:147–155.
- Austin, F., Siclari, M.J., Van Nostrand, W., Weisensel, G.N., Kottamasu, V. and Volpe, G. 1997. "Comparison of Smart Wing Concepts for Transonic Cruise Drag Reduction," *SPIE Proceedings*, 3044:33–40.
- Austin, F. and Van Nostrand, W. 1995. "Shape Control of an Adaptive Wing for Transonic Drag Reduction," *SPIE Proceedings*, 2447:45–55.
- Frecker, M. 1997. "Optimal Design of Compliant Mechanisms," PhD Dissertation, University of Michigan, Ann Arbor.
- Goldberg, D. 1989. *Genetic Algorithms in Search, Optimization, and Machine Learning*, Addison-Wesley, 1–57.
- Hetrick, J. and Kota, S. 1999. "An Energy Formulation for Parametric Size and Shape Optimization of Compliant Mechanisms," *ASME Journal of Mechanical Design*, 121:229–234.
- Joo, J. 2001. "Nonlinear Synthesis of Compliant Mechanisms: Topology and Size and Shape Design," PhD Dissertation, University of Michigan, Ann Arbor.
- Joo, J., Kota, S. and Kikuchi, N. 2001. "Nonlinear Synthesis of Compliant Mechanisms: Topology Design," *2001 ASME Design Engineering Technical Conferences*, DETC2001:MECH-14141.
- Kota, S., Hetrick, J., Li, Z. and Saggere, L. 1999. "Tailoring Unconventional Actuators Using Compliant Transmissions: Design Methods and Applications," *IEEE/ASME Transactions on Mechatronics*, 4(4):396–408.
- Martin, C.A., Jasmin, L., Flanagan, J., Appa, K. and Kudva, J.N. 1997. "Smart Wing Wind Tunnel Model Design," *SPIE Proceedings*, 3044:41–47.
- Martin, J.W., Main, J.A. and Nelson, G.C. 1998. "Shape Control of Deployable Membrane Mirrors," *ASME Adaptive Structures and Materials Systems Conference*, ad57/md83:217–223.
- Martin, J.W., Redmond, J.M., Barney, P.S., Henson, T.D., Wehlburg, J.C. and Main, J.A. 2000. "Distributed Sensing and Shape Control of Piezoelectric Bimorph Mirrors," *Journal of Intelligent Materials Systems and Structures*, 11:744–757.
- Saggere, L. and Kota, S. 1999. "Static Shape Control of Smart Structures Using Compliant Mechanisms," *AIAA Journal*, 37(5):572–578.
- Washington, G. 1996. "Smart Aperature Antennas," *Journal of Smart Materials and Structures*, 5(6):801–805.
- Webb, G.V., Lagoudas, D.C. and Kulkarni, M. 1999. "Adaptive Shape Control for an Sme-Actuated Aerofoil Rib Structure," *Proceedings of IMECE*, 59:205–212.
- Yoon, H.S. and Washington, G. 1998. "Piezoceramic Actuated Aperature Antennae," *Journal of Smart Materials and Structures*, 7(4):537–542.
- Yoon, H.S., Washington, G. and Theunissen, W.H. 2000. "Analysis and Design of Doubly Curved Piezoelectric Strip-Actuated Aperature Antennas," *IEEE Transactions on Antennas and Propagation*, 48(5):755–763.